Carbohydrate Polymers 87 (2012) 257–264

Contents lists available at ScienceDirect

Carbohydrate Polymers

journal homepage: www.elsevier.com/locate/carbpol

Transparent cellulose sheets as synthesis matrices for inorganic functional particles

Daniel Van Opdenbosch[a], Philipp Maisch[a], Gerhard Fritz-Popovski[b], Oskar Paris[b], Cordt Zollfrank[a,*]

[a] Department for Materials Science and Engineering – Glass and Ceramics, University of Erlangen–Nuremberg, Martensstraße 5, D-91058 Erlangen, Germany
[b] Institute of Physics, Montanuniversitaet Leoben, Franz Josef Straße 18, A-8700 Leoben, Austria

ARTICLE INFO

Article history:
Received 3 May 2011
Received in revised form 15 July 2011
Accepted 25 July 2011
Available online 3 August 2011

Keywords:
Cellulose sheets
Europium(III) fluoride phosphor
Photoluminescence
Transmission electron microscopy
Small angle X-ray scattering

ABSTRACT

Transparent cellulose sheets were prepared through tape-casting a solution of cellulose. Flexible, luminescent sheets were produced by adding europium trichloride to the casting solution and treating the sheets with an aqueous solution of ammonium fluoride. Scanning electron micrographs of the resulting sheets showed europium trifluoride particles with diameters from 200 nm to 500 nm. These were found by transmission electron microscopy to be agglomerates of crystallites in the size range of 10–20 nm. The structure of supercritically dried sheets was further assessed by small-angle X-ray scattering and suggests a preferred orientation of slightly elongated pores of roughly 12 nm in diameter. Evaluation of the emission characteristics of the sheets showed the band pattern between 580 nm and 700 nm typical for Eu^{3+} phosphors. Our developed process is a versatile tool for the fabrication of transparent cellulose structures with different shapes and various embedded functional particles.

1. Introduction

Cellulose is the economically and technologically most important biopolymer (Bäurich, Blechschmidt, Davydenko, Dobschall, & Fischer, 2010). It is a non-branched, syndiotactic homopolymer composed of up to 10,000 D-glucose units connected by $\beta(1\rightarrow4)$ glycosidic bonds, depending on its source (Klemm, Philip, Heinze, Heinze, & Wagenknecht, 1998). Its chemical functionality is dominated by hydroxyl groups, which are arranged in a plane in the C2, C3 positions and a methylol group at the C6 position of the glucose molecule and responsible for the cellulose's affinity for water. The cellulose molecules are stiffened and arrange into crystalline microfibril sections due to the intra- and intermolecular interactions between these hydroxyl groups (Burgert et al., 2005; Stoll & Fengel, 1977). Complete dissolution of cellulose is complicated by the spatial arrangement and interactions between cellulose molecules in natural materials (Fengel & Wegener, 1989; Pinkert, Marsh, & Pang, 2010). For this, hydrogen bridge bonds between the molecules have to be broken and the hydroxyl groups either derivatized or shielded to dissolve the molecules and keep them in solution (McCormick, Callais, & Hutchinson, 1985). The preparation of pure cellulosic products from solution can be based on the re-crystallization of dissolved cellulose in the desired spatial arrangement. Economically important examples for this approach are viscose, cellophane and celluloid (Koch, 1966; Simon, Muller, Koch, & Muller, 1998). Using regenerated cellulose as a template material allows to include a second phase in dissolved or already gelled cellulose. In the past, a number of scientifically significant gel templating methods have been published. A gel from agar, a polysaccharide similar to cellulose was used as a template for nanoscale silver particles (Ayyad, Munoz-Rojas, Oro-Sole, & Gomez-Romero, 2010). This was performed either during the formation of the gel or afterwards and led to finely dispersed nanoscale silver particles. In a similar way, finely structured silica (Jiu, Kurumada, Pei, & Tanigaki, 2004), zinc oxide (Lazarides & Gaillard, 2003) or iron oxide phases (Chang, Yu, Ma, & Anderson, 2011) structures were prepared from agar gel templates. Mannan templates were used to prepare nanostructured apatite structures (Yamane, Sugawara, Watanabe, & Akiyoshi, 2009), while starch and alginate templates were used for generating iron oxide (Nidhin, Indumathy, Sreeram, & Nair, 2008). As an alternative to polysaccharide gel templates, animal collagen and gelatin templates have been used for the synthesis of apatite materials, resulting in inorganic–organic composites with defined inorganic materials structures on a nanometer scale (Kollmann et al., 2010; Zahn, Hochrein, Kawska, Brickmann, & Kniep, 2007). Such plant- or animal-derived biological gels can serve as templating sites, either for in situ synthesis or as porous templates for diffusion-driven synthesis. The reactivity of these templates is related to their surface chemistry which can be altered through chemical treatments (Abdelmouleh et al., 2004; Belgacem & Gandini, 2005; Rowell, 2006). Cellulose, although chemically similar to the examples named above, has seldom been used in

* Corresponding author.
E-mail address: cordt.zollfrank@ww.uni-erlangen.de (C. Zollfrank).

0144-8617/$ – see front matter © 2011 Elsevier Ltd. All rights reserved.
doi:10.1016/j.carbpol.2011.07.048

regenerated form for the templating of a second phase (Ma, Xu, Sun, Li, & Jia, 2010; Nelson & Deng, 2007). Compared to syntheses in a liquid medium, this has the advantage of fixating the formed inorganic material structures in their prepared state, limiting crystal growth. They can also serve to gradually release chemicals in biochemical applications (Yamane et al., 2009). The properties of the templates themselves are interesting since they can be shaped into tough, transparent sheets (Richter, 1937; Sanderson & Maloney, 1962). Removing the template by calcination can lead to inorganic materials with a controlled porosity and function (Schattka, Shchukin, Jia, Antonietti, & Caruso, 2002; Wang, Mitchell, Prince, Atanacio, & Caruso, 2008).

Rare earth ion trifluorides such as europium trifluoride (EuF_3) exhibit interesting emission properties, recommending them for advanced optical applications (Kaminskii, 1990). A simple preparation method is their precipitation from dissolved salts (Wang, Huang, Hong, Chen, & Xue, 2006a, 2006b). In the past, rare earth trifluorides have been prepared as powders by heating oxides in fluorine gas (Tanguy, Portier, Vlasse, & Pouchard, 1972), as centimeter-sized single crystals via Czochralski technique LnF_3 (Lage, Righi, Matinaga, Gesland, & Moreira, 2004), as nanocrystalline glass ceramics from molten precursors (Chen, Wang, Zheng, Guo, Yu, & Huang, 2007), as dispersed nanometer-sized particles from precipitation (Stouwdam & van Veggel, 2002) or by hydrothermal syntheses (Li, Yang, Yang, Lian, & Lin 2008).

By combining the preparation of cellulose sheet with functional particle syntheses, one could prepare transparent, flexible cellulose sheets with embedded functional inorganic particles that are fixated by the template. In this work, the non-derivatizing solvent system of lithium chloride (LiCl) in dimethyl acetamide (DMAc) was used to prepare a cellulose solution from which sheets were cast and characterized (El Seoud, Regiani, & Frollini, 2000; Timpa & Ramey, 1989; Timpa, 1991). EuF_3 particles were synthesized within the sheets by reacting previously included europium(III) ions (Eu^{3+}) with fluoride ions (F^-) in aqueous solution. The obtained structures and luminescence properties of the resulting sheets with and without EuF_3 were characterized. The sheets containing luminescent particles could – through upscaling of the process – be used as flexible yet tough display screen e.g. for outdoor display applications.

2. Experimental

2.1. Materials

The following reagents were used without further purification: Cellulose powder (C6663-250G, Sigma–Aldrich, St. Louis, USA), Ethanol (Et, purity ≥ 99.9%, VWR, Darmstadt, D), N,N-dimethyl acetamide (DMAc, purity ≥ 99.0%, Sigma–Aldrich Chemie, Steinheim, D), lithium chloride (LiCl, purity ≥ 99.0%, Fluka, Buchs, CH), europium(III) chloride–hexahydrate ($EuCl_3{\cdot}6H_2O$, purity ≥ 99.9%, Sigma–Aldrich Chemie, Steinheim, D) and ammonium fluoride (NH_4F, purity ≥ 98.0%, Sigma–Aldrich Chemie, Steinheim, D). The principal processing steps of this work are shown in Fig. 1.

2.2. Methods

In a typical experiment, 10 g of dried cellulose powder were suspended in 200 ml of DMAc in a round-bottom flask under stirring. A cooler was attached and the mixture then heated in an oil bath to 130 °C under magnetic stirring to remove adhered water from the cellulose molecules. After 2 h, the suspension was cooled to 100 °C and 20 g of anhydrous LiCl were added. The cooler was replaced with a drying tube and the mixture cooled to room temperature

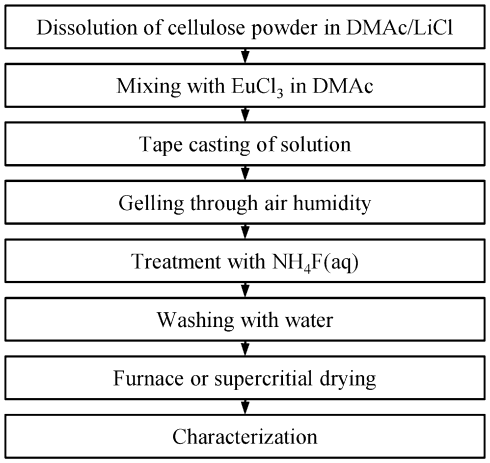

Fig. 1. Principal processing steps employed during this work.

at a rate of 10 °C/h. The controlled cooling rate was necessary to ensure a complete dissolution of the cellulose by the formation of an anhydroglucose hydroxyl group–Cl^-–Li^+ (DMAc) complex (Dawsey & McCormick, 1990; McCormick et al., 1985). An incomplete dissolution after cooling to room temperature could be remedied by cooling to 4 °C and in rare cases only by heating to 50 °C and slowly cooling to 4 °C again. The result was a clear liquid with a honey-like viscosity that could be stored without visible alteration in a sealed glass bottle for at least one month. The rheological properties of the solution were analysed using a rheometer (UDS-200, Paar Physika, Stuttgart, D) with a rotating cone-plate arrangement (MK 23, Paar Physika, Stuttgart, D) at a temperature of 20 °C. The cone radius was 25 mm and its angle was 2°; the shear rate was varied from 0.01 s^{-1} to 200 s^{-1}.

From the cellulose solution, sheets were prepared by diluting 2.5 ml of the original solution with an equal volume of DMAc and subsequent tape casting it using a manual doctor blade caster with a variable blade height set to 1 mm. Tape casting to a glass substrate resulted in the most uniform and planar cellulose sheets. The resulting layers of cellulose solution were then left to gel to sheets at either 26%, 58% or 100% relative humidity for one week. The sheets were peeled off the substrate and washed repeatedly by stirring them in 250 ml of double distilled water. The absence of chloride ions in the washing solution (silver nitrate test) indicated the completion of the purification process. Warping of the sheets was prevented by drying them between two flat cellulose filter papers for 3 d and applying a pressure of 0.1 Pa. Residual water was removed by treating the sheets with temperatures of 50 °C, 85 °C and finally 105 °C for 2 h each. Alternatively, some sheets were supercritically dried (Samdri-PVT-3D, Tousimis, Rockville, USA) to preserve the original porous structure of the templates for analyses. These sheets were fastened in the exchange chamber of the dryer with flat wire mesh to prevent warping. Dried specimens were tested for residual DMAc by Fourier-transform infrared spectroscopy (FTIR) in attenuated total reflection mode (Impact 420, Nicolet Instruments, Madison, USA with added DuraSampler, Resultec, Köln, D). Homogenous inclusion of Eu^{3+} in the sheets was achieved by preparing 2.5 ml of a saturated solution of $EuCl_3$ in DMAc, which had a molarity of 0.23 mol/l at 25 °C. This solution was mixed with an equal volume of the solution of cellulose in DMAc by stirring for 1 d. The resulting mixture consequently had an Eu^{3+} content of 0.12 mol/l. The sheets produced from this solution were then immersed in a solution of 0.2 g NH_4F in 150 ml water to provide a threefold stoichiometric excess of F^- ions for the precipitation of EuF_3. The sheets containing the precipitated inorganic

particles were washed and dried in the same way as the native cellulose sheets.

The dimensions and weights of all prepared sheets were measured. Their strut densities (ρ_{strut}) were analysed using a helium pycnometer (AccuPyc 1330, Particle and Surface Sciences, Gosford, AUS). From ρ_{geom} and ρ_{strut}, the porosities (P) of the materials were calculated by $P = 1 - \rho_{geom}/\rho_{strut}$. Thermogravimetric analysis (TGA) and differential thermal analysis (DTA) curves were simultaneously recorded for both the native cellulose and EuF_3-containing sheets in air with a heating rate of 300 °C/h on a combined TGA/DTA device (STA 409, Netzsch Gerätebau, Selb, D). Precipitates from the NH_4F treatment solution and calcined sheets were ground and spread onto the sample holder of an X-ray diffractometer (Diffraktometer D500, Siemens, Karlsruhe, D). Diffraction patterns were recorded with monochromated Cu Kα radiation, an integration time of 0.3 s, a step size of 0.02° at an acceleration voltage of 30 kV from $2\theta = 5$–70°. X-ray diagrams were analysed using a pattern analysis program (Diffracplus Eva, Bruker AXS, Karlsruhe, D). Sheets were immersed in liquid nitrogen, broken and transferred onto sample holders covered with conductive carbon paste (Leit-C, Plano, Marburg, D) and sputtered with gold for scanning electron microscopy (SEM, Quanta 200, FEI, Hillsboro, USA) and energy-dispersive X-ray (EDX) analysis (INCA x-sight TVA3, Oxford Instruments, Oxford, UK). The SEM micrographs and EDX analyses were performed at an acceleration voltage of 20 kV. Specimens embedded in Spurr's epoxy resin (Spurr, 1969) were trimmed with a steel razor blade and then sectioned with an ultramicrotome (Ultracut E, Reichert-Jung, Depew, USA). Sections with a thickness of 80 nm were transferred to carbon-coated copper grids (S160, Plano, Wetzlar, D) for transmission electron microscopy (TEM, CM30, Philips, NL) imaging using an attached charge-coupled device camera (FastScan-F114, Tietz Video and Image Processing Systems, D). TEM imaging was carried out at an acceleration voltage of 300 kV. The photoluminescence (PL) of the specimens was measured on a spectrofluorometer (Fluorolog 3, Horiba Jobin Yvon, Edison, USA), equipped with a 450 W Xenon lamp for the excitation and two f/3.6 Czeny–Turner double-grating monochromators for selecting the wavelength range of the exciting and emitted light. The excitation slit width was 5 nm, the emission slit width 1 nm and the measurement increment 1 nm. A filter with a cutoff below 400 ± 6 nm (GG400, Schott, Mainz, D) was applied to exclude the second order light emissions. Excitation spectra were measured from 300 nm to 575 nm and corrected for the spectral distribution of the lamp intensity with a photodiode reference detector starting at 240 nm. Emission and excitation spectra were also corrected for the spectral response of the monochromators and the detector, using correction spectra provided by the manufacturer. The emission spectra were measured from 550 nm to 750 nm. Combined wide- and small-angle X-ray scattering (WAXS/SAXS) measurements (Nanostar, Bruker AXS, Karlsruhe, D) were performed, with a sealed-tube X-ray generator (KFL Cu 2k, Siemens, D) using Cu Kα radiation, cross-coupled multilayer Göbel-mirrors and a 2D area detector (HiStar, Bruker AXS, D). Sample transmissions were determined by introducing glassy carbon into the direct beam and relating the scattered intensity to measurements without the sample. The detector background correction was performed by subtracting the 2D pattern acquired for the empty camera.

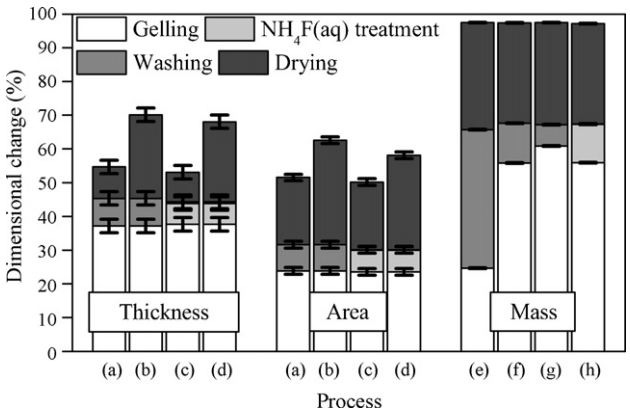

Fig. 2. Shrinkage and mass losses of sheets from different processing routes; (a) supercritically dried, (b) air-dried, (c) supercritically dried from Eu^{3+}-containing solution, (d) air-dried from Eu^{3+}-containing solution, (e) gelled in 26% humidity, (f) gelled in 58% humidity, (g) gelled in 100% humidity, and (h) Eu^{3+}-containing solution gelled in 58% humidity.

3. Results

The addition of an equal volume of DMAc to the native cellulose solution significantly reduced the viscosity of the solution. The native solution had a dynamic viscosity of 3.45 Pa s at a shear rate of 25 s^{-1}, which declined linearly to 2.9 Pa s at 200 s^{-1}. It showed a viscosity hysteresis of 0.2 Pa s (6% of the total viscosity). The diluted solution had a viscosity of 0.11 Pa s, which did not change detectably for higher shear rates. It showed a hysteresis of 0.001 Pa s (1% of the total viscosity). The relative humidity strongly influenced the speed of the cellulose gelling process. Specimens gelled in a relative humidity of 26%, 58% or 100% were strong enough to be peeled off the substrate after 7 d, 4 d or 3 d, respectively. Fig. 2 shows the shrinkages and mass loss of the sheets during processing, starting from 1 mm thickness and the individual masses of the tape-cast solutions. Sheets gelled at relative humidities of 26%, 58% and 100% experienced respective mass losses of 25%, 56% and 61%, during gelling. After the washing process, however, they all had the same total mass loss of 67%. Processing routes with $EuCl_3$ added to the diluting DMAc were treated with NH_4F dissolved in double distilled water before washing. This had the same effect on the mass loss as washing, which then had no noticeable effect. Some precipitation of EuF_3 particles in the NH_4F treatment solution due to leaching of Eu^{3+} from the sheets was observed. Supercritical drying reduced the shrinkages by about 10% but had no influence on the sheets' masses. The cellulose sheets without EuF_3 had a final mass which was 2.6% of the mass of the originally cast solution while the EuF_3-filled sheets retained 2.9% of their original mass. Specimens with or without EuF_3 gelled at the same humidity showed no difference in shrinkage. Although the sheets with EuF_3 showed slightly reduced shrinkages and mass losses, they were within the calculated measurement uncertainties. The discrepancies between the dimensional and the mass losses during processing are attributed to the formation of pores within the sheets. This was also indicated by their calculated porosities, Table 1. The strut density of the cellulose powder used as the starting material was measured to be 1.539 ± 0.004 g/cm^3. Air-dried

Table 1
Densities and porosities of the cellulose sheets as determined by geometrical and helium pycnometry measurements.

Cellulose sheet type	Geometrical density (g/cm^3)	Strut density (g/cm^3)	Calculated porosity (%)
Air-dried	1.21 ± 0.02	1.646 ± 0.005	26 ± 2
Supercritically dried	0.85 ± 0.02	1.662 ± 0.016	49 ± 3
Air-dried, with EuF_3	1.47 ± 0.03	1.823 ± 0.025	19 ± 4
Supercritically, with EuF_3	0.87 ± 0.02	1.839 ± 0.005	53 ± 2

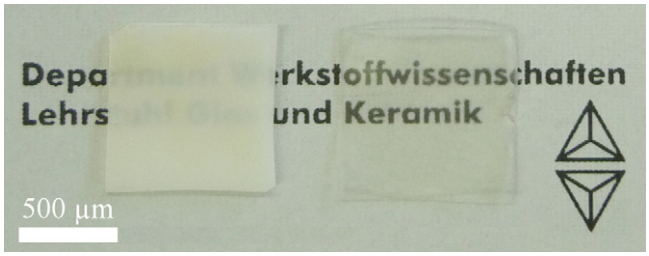

Fig. 3. Photograph of supercritically (left) and air-dried (right) cellulose sheets.

sheets were transparent while supercritically dried specimens had an opaque appearance, Fig. 3. All sheets had a good mechanical stability and could not be manually torn apart or broken by bending. In fact, they could be completely folded without being damaged.

Fig. 4 shows a representative FTIR spectrum recorded from a cellulose sheet and the spectrum of DMAc for comparison. The strongest bands from DMAc at 1632 cm^{-1} (C=O stretching), 1392 cm^{-1} (N–CH_3 deformation), 1186 cm^{-1} (C–N stretching) and 1010 cm^{-1} (C–CH_3 rocking) cannot be found in the spectra of the cellulose sheets. Here, prominent peaks can be found at 1648 cm^{-1} (water H–O–H scissoring), 1368 cm^{-1} (cellulose C–H bending), 1156 cm^{-1} (cellulose C–O–C asymmetric stretching) and 1019 cm^{-1} (cellulose C–O stretching) (Liang & Marchessault, 1959; Verbovy, Smagala, Brynda, & Fawcett, 2006).

The thermal properties from the combined TGA/DTA measurements show a similar behavior of the sheets with and without EuF_3 particles. Only 5% of their original mass is lost below 277 °C. From there to 322 °C, 44% are lost in a slightly exothermic process. The mass loss rate decreases and only 22% are lost to 437 °C. This is the onset temperature for the final, strongly exothermic mass loss of 26% for pure cellulose sheets and 24% for sheets with EuF_3. A final loss of 97.2% for pure cellulose sheets and 95.0% for EuF_3-filled sheets is observed at 514 °C. The residue of the EuF_3-cellulose sheets after heating to 800 °C was analysed by XRD and found to be a mixture of Eu_2O_3 (International Centre for Diffraction Data PDF 00-043-1008) and EuOF (PDF 00-026-0636). Considering the different molar masses of these compounds, the residue's mass gives an envelope for the amount of EuF_3 originally present within a sheet made by casting with a blade height of 1 mm between 2.5 mass% (only EuOF residue) and 2.6 mass% (only Eu_2O_3 residue). XRD patterns of the particles that formed in the NH_4F treatment solution from Eu^{3+} leaching out of the sheets showed that they were of hexagonal EuF_3 (PDF 00-032-0373).

The excitation spectra obtained by PL analysis of the EuF_3-filled sheets, Fig. 5, showed the expected bands characteristic for the intra-f energy transitions of Eu^{3+} at 316 nm ($^7F_0 \rightarrow {}^5H_3$), 360 nm ($^7F_0 \rightarrow {}^5D_4$), 375 nm ($^7F_0 \rightarrow {}^5L_7$), 394 nm ($^7F_0 \rightarrow {}^5L_6$),

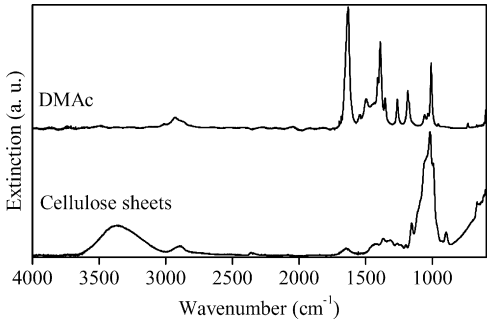

Fig. 4. FTIR spectra of the cellulose solvent DMAc and the prepared cellulose sheets.

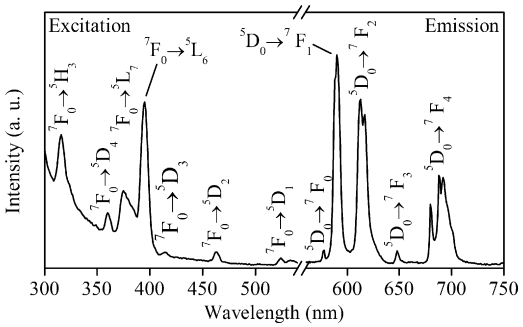

Fig. 5. PL excitation and emission spectrum of EuF_3-containing cellulose sheets.

415 nm ($^7F_0 \rightarrow {}^5D_3$), 463 nm ($^7F_0 \rightarrow {}^5D_2$) and at 524 nm ($^7F_0 \rightarrow {}^5D_1$) (Flores-Acosta, Perez-Salas, Aceves, Sotelo-Lerma, & Ramirez-Bon, 2005). The emission spectra of EuF_3 filled sheets excited at the $^7F_0 \rightarrow {}^5L_6$ band showed the characteristic sharp lines associated with the transitions between the non-degenerate $^5D_0$ state and the $^7F_{0-4}$ levels of Eu^{3+} (Buijs, Meyerink, & Blasse, 1987; Hunt & Pappalardo, 1985). The magnetic–dipole (MD) transitions at 577 nm ($^5D_0 \rightarrow {}^7F_0$), 590 nm ($^5D_0 \rightarrow {}^7F_1$) and 648 nm ($^5D_0 \rightarrow {}^7F_3$), as well as the ED transitions at 613 nm ($^5D_0 \rightarrow {}^7F_2$) and 690 nm ($^5D_0 \rightarrow {}^7F_4$) were observed. The ratio of the intensities from the $^5D_0 \rightarrow {}^7F_1$ MD bands to those of the $^5D_0 \rightarrow {}^7F_2$ ED bands, the asymmetric ratio of transitions A_{21}, is determined by integration from 580 nm to 601 nm and from 601 nm to 615 nm: $A_{21} = I_{MD}/I_{ED} = 0.89$. The sheets without EuF_3 showed no distinct luminescence bands.

The pure cellulose sheets exhibited smooth surfaces as shown from SEM micrographs taken in backscattered electron imaging mode, Fig. 6a. Inorganic particles could be distinctly discerned within the EuF_3-filled sheets, Fig. 6b. The particles were evenly distributed over the sheet plane, Fig. 6c. According to EDX analyses, these particles contained europium and fluorine, as expected. There was a difference in particle content between the sheet centers and the surfaces, where the NH_4F solution was in contact with the sheets. The particles were evenly shaped, prolate spheroids 579 ± 84 nm long and 246 ± 43 nm in diameter, as graphically determined from 50 particles. TEM micrographs showed that the particles are agglomerates, composed of primary crystallites with dimensions of 10–20 nm, Fig. 7a. This crystallite size was confirmed by HRTEM micrographs, Fig. 7b.

The SAXS analyses showed weak scattering for air-dried specimens as compared to supercritically dried ones. From the 2D scattering patterns, radial line intensity distributions were determined. Indirect Fourier transformation (Glatter, 1977) gives evidence for globular structures that might be slightly elongated. Therefore, size distributions assuming spherical shape of the particles and weighted by particle volume were computed using the indirect transformation technique (Glatter, 1980). The distribution curves of scattering structure sizes in supercritically dried sheets exhibited a maximum at a radius of 6 nm and an asymmetric curve with sizes up to 25 nm for the sheets filled with EuF_3 particles, Fig. 8. The 2D scattering patterns obtained were not circular but slightly anisotropic. The inset in Fig. 8 is an azimuthal intensity distribution function over all points from a scattering vector $q = 0.19\ nm^{-1}$ to $q = 0.38\ nm^{-1}$. From WAXS patterns, the crystallite sizes of the EuF_3 particles were estimated. This was accomplished by considering the (1 1 1) reflex, subtracting a linear background and determining the full peak width at half maximum. The crystallite sizes were calculated from the Scherrer-equation. The calculated crystallite sizes were 20 ± 10 nm, the high standard error being due to the unfavorable peak-to-background intensity ratio.

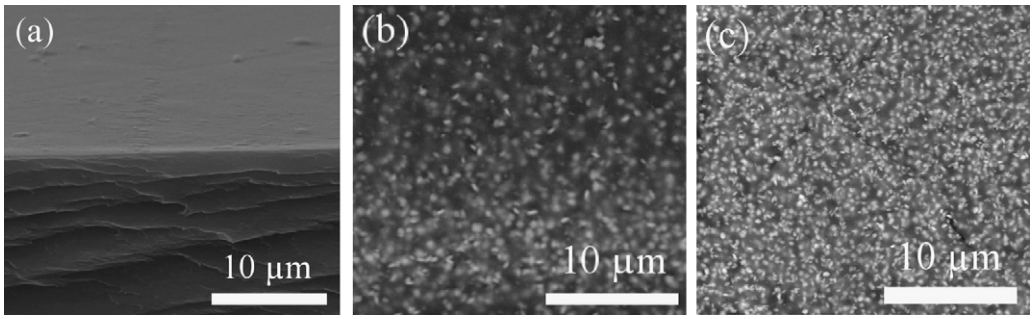

Fig. 6. SEM micrographs of 1 mm thick cellulose sheets: (a) cross-section of pure, broken in liquid nitrogen, fracture plane (bottom) and surface (top), (b) cross-section of EuF_3-filled, 0.05 mm below the surface, and (c) top view of the EuF_3-filled sheet surface.

4. Discussion

Cellulose was selected as the templating material because of the chemical and structural functionality it provides (Klemm et al., 1998). More specifically, its superior mechanical properties in relation to other biopolymers and polymers in general were crucial in the decision to use cellulose gels for the templating performed in this work (Burgert et al., 2005). The solvent system DMAc/LiCl is ideal because it is able to dissolve cellulose by complexing the hydroxyl groups without derivatization, and therefore yielding the cellulose in its original chemical state after precipitation, apart from its transition into the cellulose-II modification and polymorphs (Zugenmaier, 2001). The cellulose solutions were prepared with the maximum amount of cellulose dissolvable in a volume of DMAc in less than 1 d, which was 5 mass% before dilution (McCormick et al., 1985). The cellulose content of the diluted solution, 2.5 mass%, was roughly confirmed by the mass loss of 97.4% throughout the process starting from the tape-cast solution, Fig. 2. The cellulose solution can also be adapted for many shaping methods such as spin-coating, tape-casting, moulding or drawing by changing its viscosity. An incomplete dissolution of the cellulose is thought to be due to a too rapid cooling to room temperature. If the mixture is allowed to cool while intermolecular hydrogen bridge bonds still exist between the cellulose molecules, the complexation by the Li^+(DMAc) macrocation is sterically hindered. Therefore, prior publications stress the importance of a slow cooling process (Dawsey & McCormick, 1990; McCormick et al., 1985).

The gelling process is driven by the diffusion of water molecules into the solution, which re-form the hydrogen bond network which was interrupted by the solvent (Kondo, Togawa, & Brown, 2001). During this process, the solvent is expelled from the forming gel, leading to a reduction of both the sheets' sizes and masses through the evaporation of the water. Increased humidity leads to shorter gelling times and washing in water completes the shrinkage of the sheets. It was proposed that a mixture of distilled water and isopropyl alcohol followed by washing in running water, both "under a pressure load", is best suited to remove synthesis residue from cellulose sheets prepared from the process used in this work and to obtain films with a smoother surface structure and optimal optical transmission (Nayak, Chen, & Kim, 2008). We concluded from the FTIR analyses and silver nitrate testing that washing by stirring in periodically exchanged double distilled water is sufficient for the removal of both the DMAc and the LiCl. Although these bands from the cellulose sheets are close to those of DMAc, they had markedly different appearances and gave no indication of residual DMAc in the sheets. The ratio of the areas of the peaks at 1370 cm^{-1} and at 670 cm^{-1} was used to assess the ratio of cellulose-I to cellulose-II

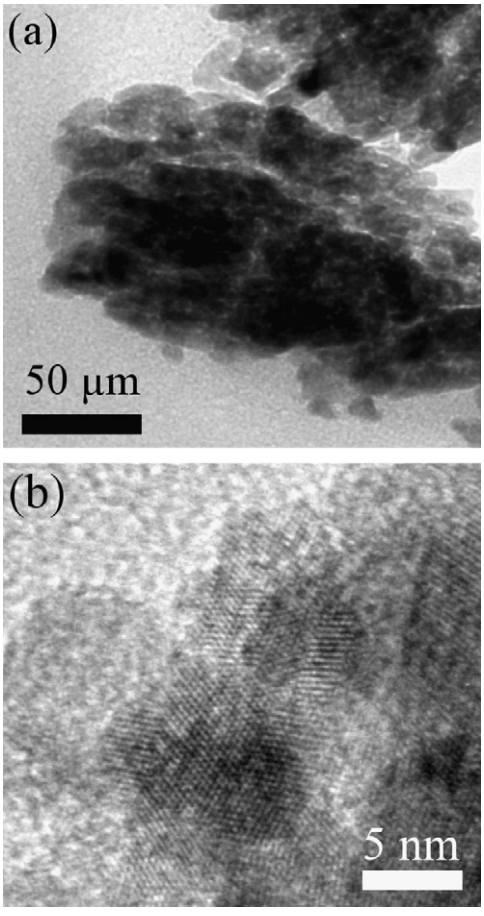

Fig. 7. TEM micrographs of (a) a cluster of EuF_3 crystallites, (b) HRTEM micrograph of EuF_3 crystallites.

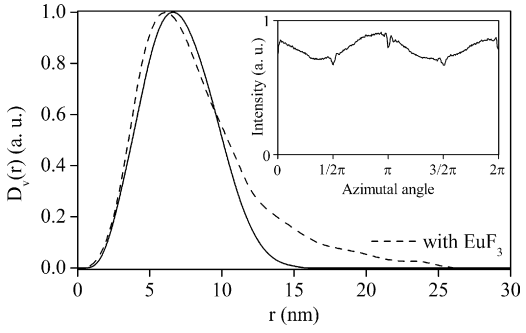

Fig. 8. Scattering structure size distribution in supercritically dried sheets over scattering structure radius r as determined by calculation from SAXS measurements; inset: azimuthal intensity distribution of the 2D scattering pattern. The drops in the curve at each quarter of a full circle are due to the strings, which held the primary-beam stopper during measurements.

in linters regenerated from sodium hydroxide (Nelson & O'Connor, 1964). Ratios from 8 to 4 were indicative of native cellulose-I and regenerated cellulose-II, respectively. From the spectra recorded in this work, ratios of 0.7 were determined after baseline subtraction similar to that performed by Nelson et al. This is a further indicator that the sheets are obtained in the cellulose-II modification.

The surfaces obtained by slow drying under a load of 0.1 Pa between sheets of filter paper did not show significant wrinkles, Fig. 6a. Since the shrinkages and mass losses after washing were the same for all sheets, gelling at ambient humidity levels, unless they are lower than 25%, is recommended as the most facile variant for the preparation of such sheets as prepared in this work. If short processing times are required, a water-enriched gelling atmosphere should be used. The difference in shrinkage between the air-dried and the supercritically dried specimens due to drying alone and attributed to non-collapsing pores is 25%. This is in agreement with the porosities calculated from ρ_{geom} and ρ_{strut}, which also show a decrease of the porosity in air-dried sheets of 23% and 34% (with EuF_3), Table 1. The increased ρ_{strut} of the EuF_3-containing sheets is due to the inclusion of the more dense ($\rho_{EuF_3} = 6.76\ \ g/cm^3$) EuF_3 particles (Batsanov, Lapshin, & Ovsyannikova, 1969). The EuF_3 content of the sheets could be calculated from Eq. (1) as 3.5 mass%. This is reasonably close to the amount of EuF_3 determined by the oxide left over after calcination and leads to the conclusion that the relative EuF_3 content by mass $n_{m(EuF_3)}$ of the sheets is between 2.5 mass% and 3.5 mass%.

$$n_{m(EuF_3)} = \frac{\rho_{strut} - \rho_{geom}}{\rho_{EuF_3} - \rho_{geom}} \quad (1)$$

The mass loss processes observed during TGA/DTA analysis of the sheets were characteristic for cellulosic materials (Beall, 1971) and could be attributed to the evaporation of adsorbed water or residual nitrogen compounds from the NH_4F treatment of the sheets at low temperatures (Branca & Di Blasi, 2003; Byrne & Nagle, 1997). The exothermic DTA signal found around 300 °C can be assigned to the transformation of the cellulose into a carbonaceous material under decomposition of the anhydrous glucose units (Beall, 1971). The second highly exothermic mass loss process at higher temperatures is due to the oxidation of this carbon (Singh, Arora, & Lal, 1996; Soares, Ricardo, Jones, & Heatley, 2001). The mass losses throughout processing found in this work were comparable to those found in literature for films washed with distilled water with isopropyl alcohol (Yun, Chen, Nayak, & Kim, 2008).

The diffusion processes of the ions from which the phosphor particles formed were bidirectional: F^- ions diffused into and Eu^{3+} ions out of the sheets. As evidenced by the SEM micrographs, EuF_3 was mainly formed in the first 5 μm below the sheet surface, which is the zone in which the ions interdiffused. Since a stoichiometric triple-excess of F^- ions was used in the treatment solution, the number of Eu^{3+} ions incorporated in the sheets is assumed to have been the limiting factor to the amount of EuF_3 formed. The observed agglomerate particle and primary crystallite sizes in the samples were similar to those found for EuF_3 prepared from aqueous solution in literature (Wang et al., 2006a, 2006b). The luminescence sheets showed high intensities from MD transitions indicative of a hexagonal EuF_3 phase (Greis & Petzel, 1973; Jayasankar, Antic-Fidancev, Blaise, & Porcher, 1986; Singh et al., 2008; Zalkin & Templeton, 1953). This was confirmed by XRD and observations in literature (Flores-Acosta et al., 2005; Krupa & Queffelec, 1997; Zhu, Liu, Meng, & Cao, 2007).

Small-angle X-ray scattering in the sheets was mainly attributed to the electron density contrast between the cellulose and pores. This interpretation is supported by three facts: (i) the air-dried specimens scattered X-rays and light less than supercritically dried ones, as observed from SAXS patterns and their highly transparent appearance; (ii) the scattering strength was similar for the cellulose sheets with and without EuF_3 particles; and (iii) the volume fraction of the pores is much larger (about 50% in supercritically dried specimens) than that of the EuF_3 (less than 1%). Indeed, a quantitative estimate of the contrast difference for structures of similar size reveals that the scattering from the pores should be dominant by a factor of 5 over the scattering from EuF_3 particles. Therefore, although the scattering structure sizes calculated from SAXS patterns relate to the EuF_3 crystallite sizes, any scattering from the crystallites would be overshadowed by the scattering effects of the pores. The size distributions shown in Fig. 8 are therefore in accordance with their interpretation as originating from the pores. The scattering curve, transformed into real space without loss of information had a progression indicative of globular scattering structures that might be slightly elongated, while the azimuthal distortion of the scattering pattern was indicative of a deviation from a globular form (Glatter & Kratky, 1982). The deviation of the structures from spherical symmetry leads to a slight overestimation of the width of the size distributions (Mittelbach & Porod, 1962). This indicates a process-derived anisotropical orientation of the pores in the sheets. The prolate EuF_3 particles are, however, randomly oriented as observed from both SEM and TEM micrographs. The pore anisotropy was therefore not translated to an orientation of the particles. TEM micrographs confirmed the crystallite sizes estimated from the WAXS patterns via the Scherrer equation, in additional agreement with the SAXS results. The high resolution images revealed the existence of elongated crystallites with an aspect ratio of up to 5 in the center of the particles and globular crystallites at the edges. This phenomenon is attributed to a directionally preferred growth of the EuF_3 which is favored for crystallites with longer growth times without additional surfactants (Li et al., 2008; Wang et al., 2006a, 2006b). Those crystallites which nucleated later, i.e. those at the particle edges are accordingly more globular.

5. Conclusions

We presented the fabrication of cellulose as flat, transparent, phosphor-particle filled sheets for further processing. We showed, at the example of the precipitation of EuF_3, that sheets made from regenerated cellulose can be readily used as templates for the synthesis and carriers of inorganic functional particles from aqueous solution. This opens new synthetic and material design routes to prepare transparent, flexible functional materials for applications in display technology, optical filters or wave-guiding components. Due to the possibility to tune the viscosity of the initial cellulose solution, a large number of well-known structuring techniques from spin-coating over dip-coating to simple sedimentation assisted casting can be employed to shape the components. Furthermore, it is proposed that the sheets can be further modified, for example by deposition of electrodes, structuring by etching or stacking of several sheets.

Acknowledgements

Financial support by the German Research Foundation (Deutsche Forschungsgemeinschaft, DFG) is gratefully acknowledged. We thank Sebastian Krolikowski (Department for Materials Science and Engineering – Glass and Ceramics, University of Erlangen–Nuremberg) for the photoluminescence spectra recorded for this work.

References

Abdelmouleh, M., Boufi, S., Belgacem, M. N., Duarte, A. P., Ben Salah, A., & Gandini, A. (2004). Modification of cellulosic fibers with functionalized silanes: Development of surface properties. *International Journal of Adhesion and Adhesives*, *24*(1), 43–54.

Ayyad, O., Munoz-Rojas, D., Oro-Sole, J., & Gomez-Romero, P. (2010). From silver nanoparticles to nanostructures through matrix chemistry. *Journal of Nanoparticle Research*, *12*(1), 337–345.

Batsanov, S. S., Lapshin, A. I., & Ovsyannikova, I. A. (1969). Effect of an explosion of a substance. Impact compression of rare-earth metal fluorides. *Zhurnal Strukturnoi Khimii*, *10*(2), 268–273.

Bäurich, C., Blechschmidt, J., Davydenko, E., Dobschall, E., & Fischer, K. (2010). *Taschenbuch der Papiertechnik*. Blechschmidt, Jürgen: Leipzig.

Beall, F. C. (1971). Differential calorimetric analysis of wood and wood components. *Wood Science and Technology*, *5*(3), 159–175.

Belgacem, M. N., & Gandini, A. (2005). Surface modification of cellulose fibres. *Polimeros: Ciencia e Tecnologia*, *15*(2), 114–121.

Branca, C., & Di Blasi, C. (2003). Global interinsic kinetics of wood oxidation. *Fuel*, *83*(1), 81–87.

Buijs, M., Meyerink, A., & Blasse, G. (1987). Energy transfer between Eu^{3+} ions in a lattice with two different crystallographic sites: Y_2O_3:Eu^{3+}, Gd_2O_3:Eu^{3+} and Eu_2O_3. *Journal of Luminescence*, *37*, 9–20.

Burgert, I., Eder, M., Fruehmann, K., Keckes, J., Fratzl, P., & Stanzl-Tschegg, S. (2005). Properties of chemically and mechanically isolated fibers of spruce (Picea abies [L.] Karst.). Part 1: Structural and chemical characterization. *Holzforschung*, *59*(2), 240–246.

Byrne, C. E., & Nagle, D. C. (1997). Carbonization of wood for advanced materials applications. *Carbon*, *35*(2), 259–266.

Chang, P. R., Yu, J., Ma, X., & Anderson, D. P. (2011). Polysaccharides as stabilizers for the synthesis of magnetic nanoparticles. *Carbohydrate Polymers*, *83*(2), 640–644.

Chen, D., Wang, Y., Zheng, K., Guo, T., Yu, Y., & Huang, P. (2007). Bright upconversion white light emission in transparent glass ceramic embedding Tm^{3+}/Er^{3+}/Yb^{3+}:beta-YF_3 nanocrystals. *Applied Physics Letters*, *91*(25), 251901–251903.

Dawsey, T. R., & McCormick, C. L. (1990). The lithium chloride/dimethylacetamide solvent for cellulose: A literature review. *Journal of Macromolecular Science, Reviews in Macromolecular Chemistry and Physics*, *C30*(3–4), 405–440.

El Seoud, O. A., Regiani, A. M., & Frollini, E. (2000). Derivatization of cellulose in homogeneous conditions: A brief review. *Natural Polymers and Agrofibers Based Composites*, 73–89.

Fengel, D., & Wegener, G. (1989). *Wood chemistry, ultrastructure, reactions*. Berlin: Walter de Gruyter.

Flores-Acosta, M., Perez-Salas, R., Aceves, R., Sotelo-Lerma, M., & Ramirez-Bon, R. (2005). Structural and photoluminescent properties of EuF_3 nanoparticles in zeolite A. *Solid State Communications*, *136*(11–12), 567–571.

Glatter, O. (1977). A new method for the evaluation of small-angle scattering data. *Journal of Applied Crystallography*, *10*, 415–421.

Glatter, O. (1980). Determination of particle-size distribution functions from small-angle scattering data by means of the indirect transformation method. *Journal of Applied Crystallography*, *13*(1), 7–11.

Glatter, O., & Kratky, O. (Eds.) (1982). *Small angle X-ray scattering*. Academic press Inc., London.

Greis, O., & Petzel, T. (1973). Structural chemistry of the rare earth trifluorides. *Zeitschrift fuer Anorganische und Allgemeine Chemie*, *403*(1), 1–22.

Hunt, R. B., & Pappalardo, R. G. (1985). Fast excited-state relaxation of Eu–Eu pairs in commercial Y_2O_3:Eu^{3+} phosphors. *Journal of Luminescence*, *34*, 133–146.

Jayasankar, C. K., Antic-Fidancev, E., Blaise, M. L., & Porcher, P. (1986). Optical properties of europium trifluoride and gadolinium trifluoride and paramagnetic susceptibility of europium trifluoride. *Physica Status Solidi B: Basic Research*, *133*(1), 345–353.

Jiu, J., Kurumada, K.-i., Pei, L., & Tanigaki, M. (2004). Syntheses of ordered mesoporous silica by new hybrid template. *Colloids and Surfaces, B: Biointerfaces*, *38*(3–4), 121–125.

Kaminskii, A. A. (1990). *Laser crystals: Their physics and properties*. Berlin: Springer.

Klemm, D., Philipp, B., Heinze, T., Heinze, U., & Wagenknecht, W. (1998). *Comprehensive cellulose chemistry*. Vol. 1. *Fundamentals and analytical methods* Wiley-VCH.

Koch, P. A. (1966). New chemical fibers. *Zeitschrift fuer die Gesamte Textilindustrie*, *68*(11), 821–830.

Kollmann, T., Simon, P., Carrillo-Cabrera, W., Braunbarth, C., Poth, T., Rosseeva, E. V., et al. (2010). Calcium phosphate–gelatin nanocomposites: Bulk preparation (shape- and phase-control), characterization, and application as dentine repair material. *Chemistry of Materials*, *22*(18), 5137–5153.

Kondo, T., Togawa, E., & Brown, R. M., Jr. (2001). "Nematic ordered cellulose": A concept of glucan chain association. *Biomacromolecules*, *2*(4), 1324–1330.

Krupa, J. C., & Queffelec, M. (1997). UV and VUV optical excitations in wide band gap materials doped with rare earth ions: 4f–5d transitions. *Journal of Alloys and Compounds*, *250*(1–2), 287–292.

Lage, M. M., Righi, A., Matinaga, F. M., Gesland, J. Y., & Moreira, R. L. (2004). Raman-spectroscopic study of lanthanide trifluorides with the beta-YF_3 structure. *Journal of Physics: Condensed Matter*, *16*(18), 3207–3218.

Lazarides, A. A., & Gaillard, J.-F. (2003). Characterization of polysaccharide templating of ZnO formation of relevance to natural processes of metal clearance. In *Abstracts of Papers, 225th ACS National Meeting* New Orleans, LA, United States, March 23–27, 2003, (p. IEC-251).

Li, C., Yang, J., Yang, P., Lian, H., & Lin, J. (2008). Hydrothermal synthesis of lanthanide fluorides LnF_3 (Ln = La to Lu) nano-/microcrystals with multiform structures and morphologies. *Chemistry of Materials*, *20*(13), 4317–4326.

Liang, C. Y., & Marchessault, R. H. (1959). Infrared spectra of crystalline polysaccharides. II. Native celluloses in the region from 640 to 1700 cm^{-1}. *Journal of Polymer Science*, *39*, 269–278.

Ma, M., Xu, F., Sun, R., Li, S., & Jia, N. (2010). *Cellulose/silver nano composite and preparation method thereof*. People's Republic of China: Beijing Forestry University., 11 pp.

McCormick, C. L., Callais, P. A., & Hutchinson, B. H., Jr. (1985). Solution studies of cellulose in lithium chloride and N,N-dimethylacetamide. *Macromolecules*, *18*(12), 2394–2401.

Mittelbach, P., & Porod, G. (1962). Small angle X-ray scattering of dilute colloids. VII. Distribution functions of triaxial ellipsoids. *Acta Physica Austriaca*, *5*(1–2), 122–147.

Nayak, J. N., Chen, Y., & Kim, J. (2008). Removal of impurities from cellulose films after their regeneration from cellulose dissolved in DMAc/LiCl solvent system. *Industrial & Engineering Chemistry Research*, *47*(5), 1702–1706.

Nelson, K., & Deng, Y. (2007). Encapsulation of inorganic particles with nanostructured cellulose. *Macromolecular Materials and Engineering*, *292*(10–11), 1158–1163.

Nelson, M. L., & O'Connor, R. T. (1964). Relation of certain infrared bands to cellulose crystallinity and crystal lattice type. II. A new infrared ratio for estimation of crystallinity in celluloses I and II. *Journal of Applied Polymer Science*, *8*(3), 1325–1341.

Nidhin, M., Indumathy, R., Sreeram, K. J., & Nair, B. U. (2008). Synthesis of iron oxide nanoparticles of narrow size distribution on polysaccharide templates. *Bulletin of Materials Science*, *31*(1), 93–96.

Pinkert, A., Marsh, K. N., & Pang, S. (2010). Reflections on the solubility of cellulose. *Industrial & Engineering Chemistry Research*, *49*(22), 11121–11130.

Richter, G. A. (1937). *Transparent sheet material*. Brown Co.

Rowell, R. M. (2006). Chemical modification of wood: A short review. *Wood Material Science and Engineering*, *1*(1), 29–33.

Sanderson, E. G., & Maloney, M. A. (1962). *Regenerated cellulose sheets or films*. British Cellophane Ltd., 4 pp.

Schattka, J. H., Shchukin, D. G., Jia, J., Antonietti, M., & Caruso, R. A. (2002). Photocatalytic activities of porous titania and titania/zirconia structures formed by using a polymer gel templating technique. *Chemistry of Materials*, *14*(12), 5103–5108.

Simon, J., Muller, H. P., Koch, R., & Muller, V. (1998). Thermoplastic and biodegradable polymers of cellulose. *Polymer Degradation and Stability*, *59*(1–3), 107–115.

Singh, L. R., Ningthoujam, R. S., Sudarsan, V., Srivastava, I., Singh, S. D., Dey, G. K., et al. (2008). Luminescence study on Eu^{3+} doped Y_2O_3 nanoparticles: Particle size, concentration and core–shell formation effects. *Nanotechnology*, *19*(5), 1–8.

Singh, R., Arora, S., & Lal, K. (1996). Thermal and spectral studies on cellulose modified with various cresyldichlorothiophosphates. *Thermochimica Acta*, *289*(1), 9–21.

Soares, S., Ricardo, N. M. P. S., Jones, S., & Heatley, F. (2001). High temperature thermal degradation of cellulose in air studied using FTIR and 1H and 13C solid-state NMR. *European Polymer Journal*, *37*(4), 737–745.

Spurr, A. R. (1969). A low-viscosity epoxy resin embedding medium for electron microscopy. *Journal of Ultrastructure Research*, *26*(1–2), 31–43.

Stoll, M., & Fengel, D. (1977). Studies on holocellulose and alpha-cellulose from spruce wood using cryo-ultramicrotomy I. Structural changes of the fiber walls during delignification and alkali extraction. *Wood Science and Technology*, *11*(4), 265–274.

Stouwdam, J. W., & van Veggel, F. C. J. M. (2002). Near-infrared emission of redispersible Er^{3+} Nd^{3+}, and Ho^{3+} doped LaF_3 nanoparticles. *Nano Letters*, *2*(7), 733–737.

Tanguy, B., Portier, J., Vlasse, M., & Pouchard, M. (1972). Nonstoichiometry of europium fluorides. *Bulletin de la Societe Chimique de France*, *3*, 946–950.

Timpa, J. D. (1991). Application of size exclusion chromatography for characterization of cotton fiber. *Polymeric Materials Science and Engineering*, *65*, 67.

Timpa, J. D., & Ramey, H. H., Jr. (1989). Molecular characterization of three cotton varieties. *Textile Research Journal*, *59*(11), 661–664.

Verbovy, D. M., Smagala, T. G., Brynda, M. A., & Fawcett, W. R. (2006). A FTIR study of ion-solvent interactions in N,N-dimethylacetamide. *Journal of Molecular Liquids*, *129*(1–2), 13–17.

Wang, M., Huang, Q.-L., Hong, J.-M., Chen, X.-T., & Xue, Z.-L. (2006a). Controlled synthesis and characterization of nanostructured EuF_3 with different crystalline phases and morphologies. *Crystal Growth & Design*, *6*(9), 2169–2173.

Wang, M., Huang, Q.-L., Hong, J.-M., Chen, X.-T., & Xue, Z.-L. (2006b). Selective synthesis and characterization of nanocrystalline EuF_3 with orthorhombic and hexagonal structures. *Crystal Growth & Design*, *6*(8), 1972–1974.

Wang, X., Mitchell, D. R. G., Prince, K., Atanacio, A. J., & Caruso, R. A. (2008). Gold nanoparticle incorporation into porous titania networks using an agarose gel templating technique for photocatalytic applications. *Chemistry of Materials*, *20*(12), 3917–3926.

Yamane, S., Sugawara, A., Watanabe, A., & Akiyoshi, K. (2009). Hybrid nanoapatite by polysaccharide nanogel-templated mineralization. *Journal of Bioactive and Compatible Polymers*, *24*(2), 151–168.

Yun, S., Chen, Y., Nayak, J. N., & Kim, J. (2008). Effect of solvent mixture on properties and performance of electro-active paper made with regenerated cellulose. *Sensors and Actuators B: Chemical*, *B129*(2), 652–658.

Zahn, D., Hochrein, O., Kawska, A., Brickmann, J., & Kniep, R. (2007). Towards an atomistic understanding of apatite-collagen biomaterials: Linking molecular simulation studies of complex-, crystal- and composite-formation to experimental findings. *Journal of Materials Science*, *42*(21), 8966–8973.

Zalkin, A., & Templeton, D. H. (1953). The crystal structures of yttrium fluoride and related compounds. *Journal of the American Chemical Society*, *75*, 2453–2458.

Zhu, L., Liu, X., Meng, J., & Cao, X. (2007). Facile sonochemical synthesis of single-crystalline europium fluorine with novel nanostructure. *Crystal Growth & Design*, *7*(12), 2505–2511.

Zugenmaier, P. (2001). Conformation and packing of various crystalline cellulose fibers. *Progress in Polymer Science*, *26*(9), 1341–1417.